ACS OMEGA

http://pubs.acs.org/journal/acsodf

Article

Thermal Analysis of Benzotriazolium Perrhenate and Its Implication to Rhenium Metal

James Louis-Jean,* Harry Jang, Andrew J. Swift, and Frederic Poineau*

Cite This: *ACS Omega* 2021, 6, 26672−26679

Read Online

ACCESS | Metrics & More | Article Recommendations | Supporting Information

ABSTRACT: The thermal analysis behavior of $C_6H_6N_3[ReO_4]$ was studied by simultaneous thermal gravimetric analysis (TGA) and differential scanning calorimetry (DSC) up to 700 °C under argon. Such analysis afforded rhenium metal, which was characterized by powder X-ray diffraction (PXRD), scanning electron microscopy (SEM), and energy-dispersive X-ray (EDX) spectroscopy. XRD peak broadening due to crystallite size and lattice strain was analyzed by both Williamson−Hall (W−H) and Debye−Scherrer (D−S) methods. Efforts to isolate Re metal from the thermal treatment of benzotriazole (BTA = $C_6H_5N_3$) with NH_4ReO_4 and Re_2O_7 under various atmospheres and temperatures are also reported. The results provide a significant insight into the chemistry of group VII transition metals, investigate the potential use of benzotriazole as a reducing agent for metal productions, and demonstrate a successful convenient method for rhenium metal production, which could be applied to other refractory metals.

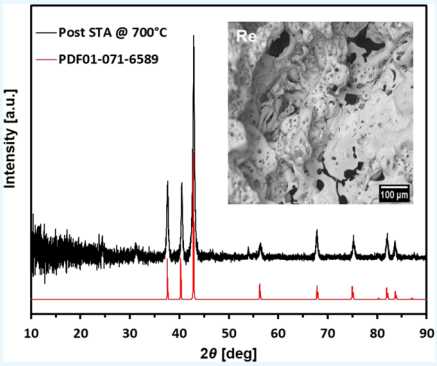

INTRODUCTION

Rhenium is among the least abundant element in the Earth's crust. However, the remarkable properties of rhenium (e.g., high melting point and corrosion resistance) and its naturally occurring isotopes (e.g., $^{187}Re/^{187}Os$ ratio[1,2] for geological dating) allow the element to find application in various technological fields.[3−5] The element is obtained from the process and purification of certain mineral concentrates (e.g., molybdenites, gadolinite, and copper-porphyry deposit).[4,6] Noddack, Tacke, and Berg are credited for the discovery of the element as they were able to recover 1 g of rhenium by processing 660 kg of molybdenite ores in 1925.[6−8] Such ores remain as the essential source of rhenium for commercial and industrial use. During the pyrometallurgical roasting process of molybdenite ores containing rhenium, solid molybdenum trioxide and volatile dirhenium heptoxide species are produced. These Re_2O_7 species pass into effluent gases and are recovered by wet scrubbing or leaching with water. In water, Re_2O_7 is converted to perrhenic acid, $HReO_4$, and various forms of perrhenate salts can be precipitated and crystallized.[9] Ammonium perrhenate (APR, $NH_4[ReO_4]$) and alkali metal derivatives remain as the most readily available forms of perrhenate salts for commercial use.

Encouraged by the various properties of 1H-benzotriazole (BTA = $C_6H_5N_3$), which undergoes protonation in aqueous media and exhibits anticorrosion properties, we further investigate the chemistry of $C_6H_6N_3[ReO_4]$ while providing a thermochemical process for producing rhenium metal. Currently, primary industrial methods for rhenium metal production are based on the reduction of APR or $K[ReO_4]$ (PPR) with hydrogen at elevated temperatures.[10−12] Hydrogen reduction of PPR, however, is found to be problematic due to impurities (e.g., potassium hydroxide), which prevent satisfactory sintering conditions. Meanwhile, the hydrogen reduction of APR remains as an effective process for rhenium metal production. Such process[11,13−15] can be achieved in a multistage decomposition, where (1) APR salt is heated in air to produce Re_2O_7, (2) conversion of Re_2O_7 to perrhenic acid, $H[ReO_4]$, followed by ion exchange to remove cation impurities, (3) precipitation of APR, and (4) decomposition of APR under hydrogen.

To minimize the number of steps for rhenium metal production, we present a new convenient method to produce Re metal. This method is based on the use of benzotriazole, $C_6H_5N_3$, as a reducing agent for metal production. This process involves the precipitation of benzotriazolium perrhenate, $HBTA[ReO_4]$ salt (benzotriazolium perrhenate (BPR)), followed by the thermal decomposition of the salt under argon. The resulting Re metal was characterized by powder X-ray diffraction (PXRD), scanning electron microscopy (SEM), and energy-dispersive X-ray (EDX) spectroscopy for structural and morphological studies. The results of this study provide a significant insight into the chemistry of group VII transition metals, investigate the potential use of benzotriazole as a

Received: July 31, 2021
Accepted: September 16, 2021
Published: September 30, 2021

reducing agent for metal productions, and demonstrate a successful convenient method for rhenium metal production.

RESULTS AND DISCUSSION

Benzotriazolium Perrhenate (BPR). The $C_6H_6N_3[ReO_4]$ salt crystallizes in the monoclinic space group $P2_1/c$ (a = 12.854(2) Å; b = 4.9121(8) Å; c = 14.819(2) Å) and its structure is stabilized by hydrogen bonds.[16,17] In BPR, tetrahedral $[ReO_4]^-$ anions are slightly distorted and neighboring anions exhibit van der Waals interaction, which form chains of Re—O1···Re—O1 along the crystallographic b-axis. White needlelike BPR is air-stable and can be stored for months without apparent decomposition. A recent analysis (experimental and theoretical)[16] indicated that the behavior of BPR in solution is governed by the nature of benzotriazole species (e. g., $C_6H_6N_3^+$, $C_6H_4N_3^-$) and solvent pK_a (Figure 1).

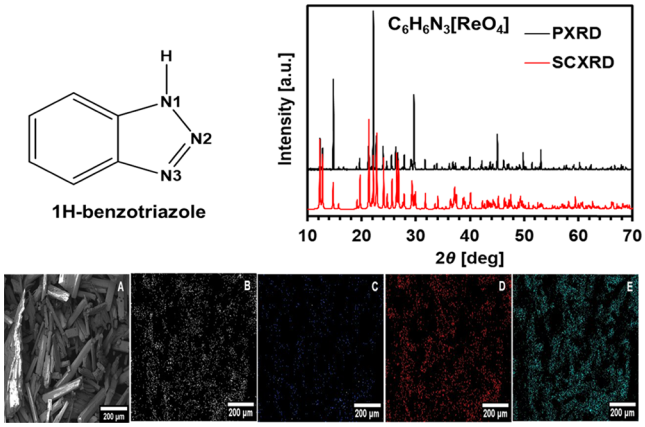

Figure 1. Left: Molecular structure of 1H-benzotriazole (BTA = $C_6H_5N_3$). Right: X-ray powder diffraction pattern (black trace) for $C_6H_6N_3[ReO_4]$ in the range 10−70° at room temperature and simulation (red trace) from single-crystal data at 100 K (−173 °C). Bottom: SEM images showing the morphology of $C_6H_6N_3[ReO_4]$ (A) and EDS mappings showing the elemental composition of carbon (B), nitrogen (C), oxygen (D), and rhenium (E).

Reduction of Perrhenate. The decomposition of ammonium perrhenate (APR) follows a series of steps involving various rhenium oxides. This includes volatile Re_2O_7, ReO_3, and ReO_2 based on the vapor pressure and temperatures of the corresponding oxides. Due to their thermodynamic differences, the high valent Re_2O_7 with a boiling point of 361.85 °C (635 K) is much easier to volatilize compared to the low-valent ReO_3 and ReO_2 with boiling points of 613.85 °C (887 K) and 1362.85 °C (1636 K), respectively.[18] In this study, the TGA of APR under argon at various heating rates lead to the formation of ReO_2 at around 400 °C, which corresponds to nearly 10% mass loss (Figure S1). Previous analyses on the study of APR to rhenium metal are reported in the literature[19] in which the metal is achieved in reductive hydrogen atmosphere through indirect processes (APR to ReO_x to Re metal) or a one-step process (APR to Re metal), as shown in the equation below.

$$NH_4ReO_{4(g)} + 7/2H_{2(g)} \rightarrow Re_{(s)} + NH_{3(g)} + 4\,H_2O_{(g)} \quad (1)$$

To minimize the steps to produce rhenium metal, this study investigates a method for the decomposition of perrhenate to Re metal without the need for hydrogen gas as a reductant. The present method relies on the various properties of benzotriazole (BTA), which for the first time has been shown to act as a reductant for metal production. This heterocyclic compound has a melting and boiling point of 100 and 350 °C, respectively.[20]

To better understand the reaction mechanism, the decomposition of benzotriazolium perrhenate was studied in triplicate using simultaneous thermal gravimetric analysis (TGA) and differential scanning calorimetry (DSC). The TGA thermogram of the salt presents a double-stage decomposition (Figure 2). The first mass loss, about 10%

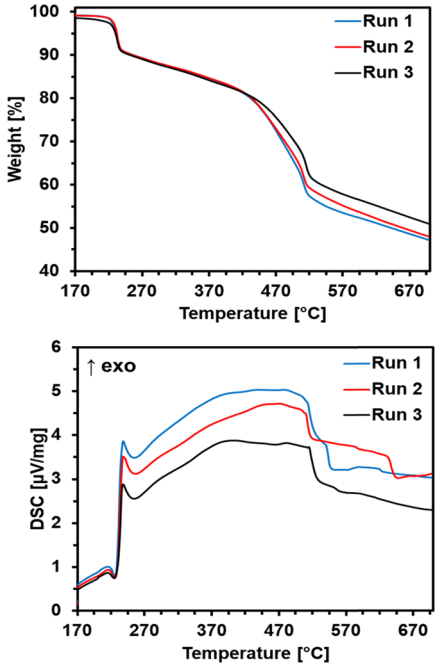

Figure 2. Simultaneous TGA (top) and DSC (bottom) analyses of triplicate $C_6H_6N_3[ReO_4]$ at 10 Kpm in argon.

from the original weight, is observed at around 243 °C, which corresponds to a strong exothermic behavior of the salt as observed in the DSC. This mass loss occurs at a temperature above the melting point (100 °C) of benzotriazole but within the temperature region of its boiling point (350 °C). The second decomposition stage begins at around 400 °C and yields to the formation of Re metal around 500 °C, which shows a broad exothermic peak in the corresponding DSC thermogram. Efforts to study the structure of the intermediate products formed about 240 °C were unsuccessful. At such temperature, the PXRD showed the material to be in a nanocrystalline or amorphous state (Figure 3); only one single diffraction peak (2θ = 28.08405°) is observed above background. Another simultaneous TGA/DSC experiment at 250 °C resulted in a nanocrystalline material. The isolated material was characterized by PXRD, which showed very-low-intensity diffraction peaks. Nonetheless, the diffraction pattern (Figure 3) showed similar peaks when compared to NH_4ReO_4 (PDF# 01-085-0347) and $HReO_4{\cdot}H_2O$ (PDF# 01-080-0049). These analyses showed the stability of $[ReO_4]^-$ within these temperature regions and that the reduction of Re(vii) occurred above 250 °C.

Considering the simultaneous thermal analyses of benzotriazolium perrhenate (Figure 2), we propose that the reduction of perrhenate to Re metal involves two separate

https://doi.org/10.1021/acsomega.1c04093
ACS Omega 2021, 6, 26672−26679

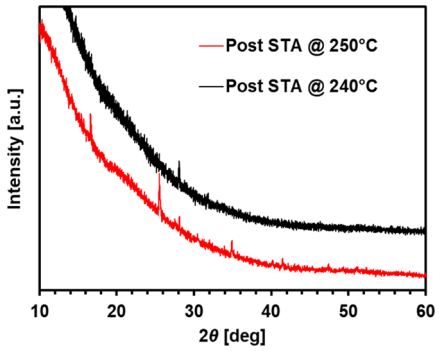

Figure 3. PXRD investigation of intermediate products formed during the simultaneous thermal analysis (STA) of $C_6H_6N_3[ReO_4]$ to Re metal showing amorphous material at 240 °C (black trace) and crystalline material at 250 °C.

reduction steps. First, $[ReO_4]^-$ is reduced to ReO_2 around 300 °C under a dry Ar atmosphere. The presence of benzotriazolium, organic cation, leads to the evolution of N_2, CO, H_2 gases and various hydrocarbon species,[21−23] which subsequently participate in the reduction of ReO_2 to rhenium metal. A carbothermic reaction with ReO_2 could also be possible given the tendency of benzotriazole to carbonize at high temperatures as observed on the surface of Al_2O_3 material.[21] In previous studies, CO and H_2 gases were used as reducing agents for metal production.[22] Therefore, the reduction to Re metal can occur by the following reactions with evolved CO and H_2 gases

$$ReO_{2(s)} + 2\,CO \rightarrow Re_{(s)} + 2\,CO_{2(g)} \quad (2)$$

$$ReO_{2(s)} + 2\,H_{2(g)} \rightarrow Re_{(s)} + 2\,H_2O_{(g)} \quad (3)$$

Morphology Study. SEM image analyses clearly show the morphological differences of rod/needlelike $C_6H_6N_3[ReO_4]$ shape pre-TGA (Figure 1) and the porous material at 750 °C post-TGA (Figure 4). Following the simultaneous thermal analysis of $C_6H_6N_3[ReO_4]$, the resulted char residue appeared as a highly charged dark-gray flaky material to the naked eyes. Initially, the samples were assumed to be of ReO_x. SEM/EDX characterization of the decomposed products did not necessarily reveal the material to be of metallic rhenium, possibly due to the difficulty in the quantification of low-Z (oxygen) atoms and interferences from the carbon tape background.

From the SEM images of thermally treated samples, it was observed that the samples are not flaky as previously thought. The materials have a silky-type texture with micron-size pores distributed on the surface. Figure 4 shows the morphology of porous Re metal obtained from this study. SEM image analyses using ImageJ software show the average area and diameter of pores to be 12.28 ± 5.78 μm^2 and 11.32 ± 5.77 μm, respectively. The porous shape of the material could be the result of the boiling or volatilization of gaseous atoms during the thermal treatment of BPR to Re metal. Since the diffusion rate of gaseous atoms increases at higher temperatures, we speculate that the porosity of the decomposed product would follow a similar trend. In this context, resulted products from higher decomposition temperature (above the temperature from this study) and/or a faster heating rate are expected to have higher porosity and thus flaky. This behavior has been previously observed in the decomposition of APR at various temperatures.[19]

Crystallographic Study. Since the SEM showed the final product as a porous material, we expected a lattice strain, weaker intensity, and broad peaks in the crystalline structure of the material. However, the powder XRD characterization of the thermally treated product of BPR showed very well-defined diffraction peaks and indicated the product to be a single phase. The powder XRD analysis of the decomposed product confirmed the material as Re metal. The presence of rhenium nitrides or carbides was not observed in the XRD pattern. Of a note, previous thermodynamic analyses have shown that rhenium is resistant to forming carbides.[24] For this reason, carburized rhenium filaments are used extensively in thermal ionization mass spectrometry for isotopic and forensic analyses since carburized rhenium filaments have higher ionization efficiency compared to noncarburized filaments.

The phase purity, crystallinity, and lattice strain of the resulted Re metal from this study were examined by powder X-ray diffraction. The PXRD pattern is presented in Figure 5. As

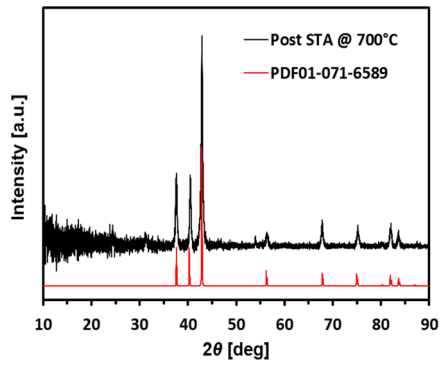

Figure 5. X-ray powder diffraction patterns for rhenium metal (black trace) post simultaneous thermal analysis of $C_6H_6N_3[ReO_4]$ in argon at 700 °C and (red trace) pattern reference number PDF01-071-6589.

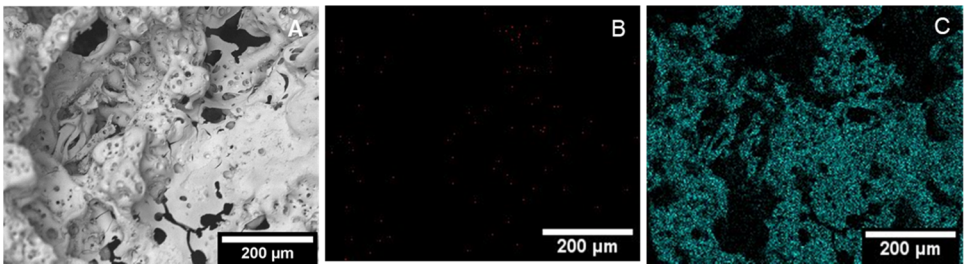

Figure 4. SEM image showing the morphology of $C_6H_6N_3[ReO_4]$ post simultaneous thermal analysis (A) yielded to rhenium metal. EDS mappings showing the elemental composition of oxygen (B) and rhenium (C).

https://doi.org/10.1021/acsomega.1c04093
ACS Omega 2021, 6, 26672−26679

witnessed in the figure, the PXRD pattern illustrates sharp detectable peaks, even smaller peaks at higher 2θ angles, and matches precisely with that of the XRD pattern reference number PDF# 01-071-6589. We speculate that peaks at around 24.409, 31.309, and 53.972° (2-theta angles), as observed in the experimental pattern, are possibly due to oxide impurities, sample textured/thickness, the distribution of sample on the XRD sample holder, and possibly the signal-to-noise ratio of the instrument. Nonetheless, the pattern is indexed on a hexagonal space group *P*63/*mmc* and reflects the presence of pure rhenium metal. Given the relatively low concentration of rhenium in nature and the high demand for its consumption, this method could be potentially deployed to recover rhenium metal from spent rhenium materials.[25,26]

In PXRD, the broadening (β_T) of peaks is due to the combined effect of crystallite size (β_D) and micro strain (β_ε). Therefore, total peak broadening can be expressed as

$$\beta_T = \beta_D + \beta_\varepsilon \tag{4}$$

Considering the broadening of X-ray diffraction peaks, the crystallite size and lattice strain can be calculated using the full width at half-maximum (FWHM) of all individual peaks.[27,28] Various methods to estimate crystallite size and lattice strain are available in the literature.[29] However, the Williamson and Hall (W−H) method remains the most used.[30] Using the Debye−Scherrer method, the average crystallite size can be calculated using the following equation.

$$D = \frac{K\lambda}{\beta_D \cos\theta} \tag{5}$$

where D is the crystallite size, λ is the wavelength of the X-ray source, and K is the shape factor. Moreover, θ and β_D are the diffraction angle (peak position) and the broadening of the peak at FHWM, respectively, in radians.

To evaluate peak broadening due to lattice strain, we used the following equation

$$\beta_\varepsilon = 4\,\varepsilon \tan\theta \tag{6}$$

where β_ε is broadening due to strain, ε is the strain, and θ is the peak position in radians. Consequently, the summation of eqs 5 and 6 leads to the W−H equation given by

$$\beta_T = \frac{k\lambda}{D \cos\theta} + 4\,\varepsilon \tan\theta \tag{7}$$

Since $\tan\theta = \sin\theta/\cos\theta$, the above equation can be rearranged and expressed as

$$\beta_T \cos\theta = \varepsilon\, 4 \sin\theta + \frac{k\lambda}{D} \tag{8}$$

This equation represents a straight line in which the slope and y-intercept are given by ε and $k\lambda/D$, respectively. Subsequently, the extracted slope and intercept from the linear fit are the strain and crystallite size, respectively. From the data displayed in Table 1, Williamson and Hall plot (W−H) for rhenium metal obtained from the simultaneous TGA/DSC is shown in Figure 6. The figure depicts a plot of 4 sin θ versus β cos θ and its fitting line. The linear fit of the scattered data allows us to calculate the strain of the material from the slope of the fit and the crystallite size from the y-intercept. The strain is given as 1.79E-4. Since the y-intercept (0.006877) is equal to $k\lambda/D$, the crystallite size (D) is calculated to be 20.16 nm. Using the Debye−Scherrer method, the average crystallite size, using eq 5, is found to be 21.38 nm, which is within the range of size obtained using the W−H method. Note that a shape factor (k) of 0.89 is considered in this calculation for this hexagonal system. A variation of this constant is discussed in ref 31.

Table 1. Profile Fitting from the PXRD of Rhenium Metal Obtained Post Simultaneous TGA/DSC of $C_6H_6N_3[ReO_4]$

2θ	d spacing	FWHM	β cos θ	4 sin θ	$k\lambda/\beta$ cos θ
24.4432	3.6406	0.0059	0.0058	0.8468	23.8282
31.2557	2.8609	0.0073	0.0070	1.0776	19.4841
37.6091	2.3909	0.0069	0.0065	1.2894	20.9555
40.5054	2.2263	0.0059	0.0056	1.3846	24.5693
42.9105	2.1070	0.0078	0.0072	1.4631	18.9357
56.3956	1.6310	0.0101	0.0089	1.8901	15.4297
67.8128	1.3815	0.0079	0.0066	2.2314	20.8881
75.2373	1.2625	0.0087	0.0069	2.4416	19.9202
82.0045	1.1746	0.0079	0.0059	2.6244	23.1337
83.6371	1.1557	0.0069	0.0051	2.6671	26.6295

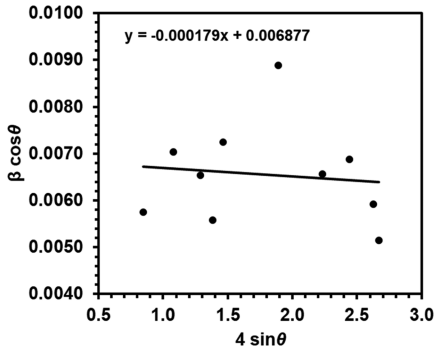

Figure 6. Williamson and Hall plot with a linear fit for Re metal obtained post simultaneous thermal analysis of $C_6H_6N_3[ReO_4]$.

Material Recovery. The method developed from the simultaneous TGA and DSC was optimized for the production and recovery of rhenium metal. To investigate the formation of Re metal from the thermal treatment of $C_6H_6N_3[ReO_4]$, BPR, 160.9 mg of the material was placed in a 5 mL alumina boat and loaded inside a quartz tube and placed in a tube furnace (Barnstead-Thermolyne 1100).

The quartz tube was connected in one end to a bubbler containing 200 mL of deionized H_2O and 20 mL of H_2O_2. This basic solution was used to trap any volatile rhenium species (e.g., Re_2O_7). The other end of the quartz tube was connected to an argon (Ar) gas tank (Figure 7). Prior to thermal treatment at 700 °C, the system was flushed with Ar for 15 min.

During the thermal treatment, the evolution of smoke fume was observed from the bubbler when the furnace reached around 400 °C. This further proved the exothermic nature of the process, as shown in the DSC thermogram. For the purpose of analysis, the recovered product in a boat is labeled as Re Metal 1, and its characterization by PXRD shows the material to be semicrystalline, as shown in Figure 8. Efforts to improve the crystallinity of the material were investigated at a higher temperature (900 °C) for 30 and 240 min, separately. While the crystallinity of the resulted metal was improved, the intensity of X-ray diffraction peaks remained low (Table 2).

Further investigations revealed that the metal could also be obtained from a 5:1 mol ratio of a powder mixture of benzotriazole and Re_2O_7 at 350 °C for 30 min under argon.

https://doi.org/10.1021/acsomega.1c04093
ACS Omega 2021, 6, 26672−26679

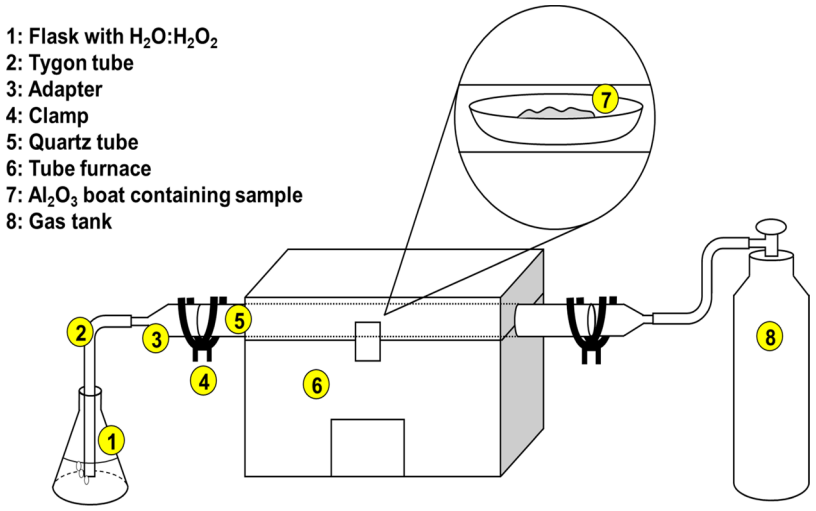

Figure 7. Experimental setup used for the preparation of Re metal using a tube furnace.

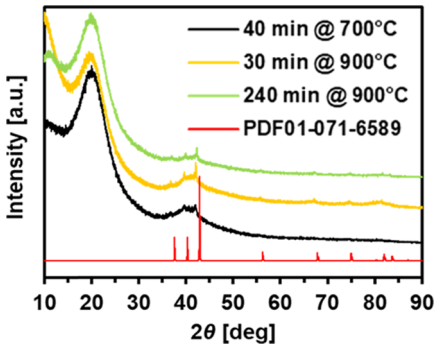

Figure 8. X-ray powder diffraction patterns for rhenium metal 1 followed by crystallization at 900 °C.

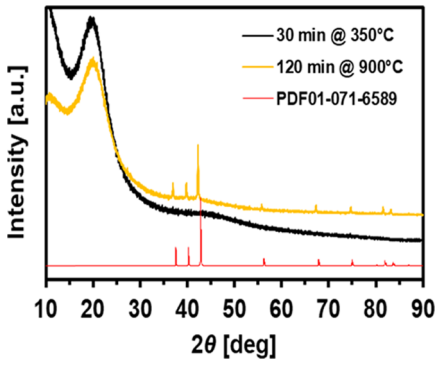

Figure 9. X-ray powder diffraction patterns for amorphous rhenium metal 2 (black trace) and crystallite rhenium metal 2a (yellow trace).

Table 2. Summary of Rhenium Metal Production at Various Thermal and Atmosphere Conditions[a]

Re metal	composite	temp [°C]	time [min]	atmosphere	note
	$C_6H_6N_3[ReO_4]$	700	40	O_2	Volatilized
1	$C_6H_6N_3[ReO_4]$	700	40	Ar	crystalline
1a	$C_6H_6N_3[ReO_4]$	900	30	Ar	crystalline
1b	$C_6H_6N_3[ReO_4]$	900	240	Ar	crystalline
2	$C_6H_5N_3$:Re_2O_7	350	30	Ar	amorphous
2a	$C_6H_5N_3$:Re_2O_7	900	120	Ar	crystalline
3	$C_6H_5N_3$:NH_4ReO_4	500	40	Ar	ReO_2
3a	$C_6H_5N_3$:NH_4ReO_4	700	60	Ar	crystalline
4	$C_6H_6N_3[ReO_4]$	350	30	N_2	amorphous
4a	$C_6H_6N_3[ReO_4]$	700	60	N_2	crystalline
5	$C_6H_6N_3[ReO_4]$	700	60	H_2	crystalline

[a]Mol ratios of all powdered mixtures are reported in the text.

This method afforded the recovery of amorphous Re metal (labeled as Re metal 2), as shown by PXRD (Figure 9). This amorphous Re metal was thermally treated at 900 °C for 240 min. This method resulted in a very shiny gray material labeled as a Re metal 2a, which is characterized by PXRD as pure Re metal (Figure 9).

We also investigated the production of Re metal from a 1:1 mol ratio of a powder mixture of benzotriazole and NH_4ReO_4 at 500 °C for 40 min under argon. This resulted in a dark-gray material. Initially, the material was assumed to be Re metal since it physically behaved similarly to previous Re metals obtained in this study. However, PXRD (Figure 10) showed the recovery material to be tetragonal ReO_2 (PDF00-055-0412). This tetragonal phase has been previously obtained from the decomposition of perrhenate in an Ar atmosphere.[32]

XRD peaks indicative to Re metal or to other Re oxides were not observed in the diffractogram. Note that the temperature profile described above was based on the simultaneous TGA/DSC of the above mixture, as shown in Figure S4. Considering that an increase of benzotriazole content could drive the formation of Re metal, we investigated a 1:5 mol ratio of a powder mixture of benzotriazole and NH_4ReO_4 at 700 °C for 60 min. This method led to the formation of shiny gray material labeled as Re metal 3a. The PXRD of this material (Figure 10) shows the existence of pure Re metal in contrast to the 1:1 mol ratio, which yielded pure tetragonal ReO_2. This analysis further proved the application of benzotriazole for Re metal production.

The thermal behavior of benzotriazolium perrhenate was also studied separately under nitrogen, hydrogen (5%), and oxygen atmospheres. Under oxygen, 149.4 mg of the salt completely volatilized at 700 °C, which resulted in the formation of dark char organic residue, a red and teal color material on both ends of the tubes just outside the furnace (Figure 11). The formation of these oxides materials have previously been observed for the technetium congener[33−36] during the oxidation of TcO_2 with O_2 at 450 °C.

https://doi.org/10.1021/acsomega.1c04093
ACS Omega 2021, 6, 26672−26679

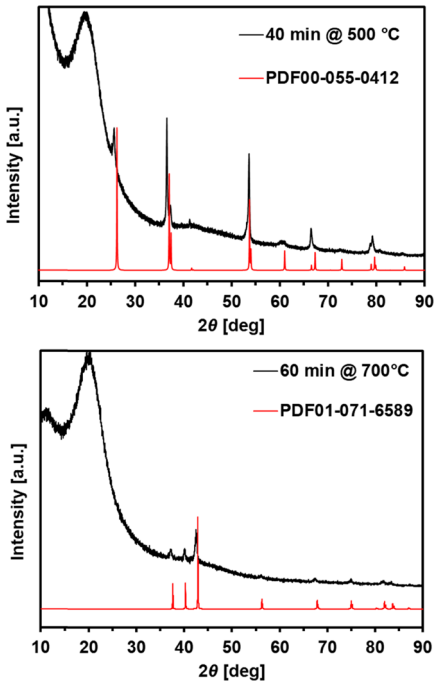

Figure 10. X-ray powder diffraction patterns showing the formation of ReO_2 from 1:1 mol ratio of NH_4ReO_4 and benzotriazole (top) and formation of Re metal from a 1:5 mol ratio of NH_4ReO_4 and benzotriazole (bottom) in an argon atmosphere.

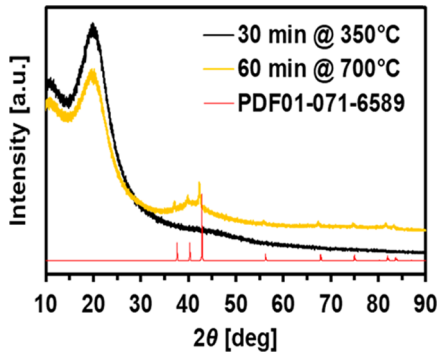

Figure 12. X-ray powder diffraction patterns for rhenium metal 4 obtained under nitrogen at 350 °C (amorphous) followed by crystallization at 700 °C.

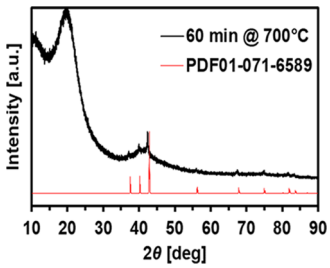

Figure 13. X-ray powder diffraction patterns for rhenium metal 5 obtained at 700 °C in a hydrogen atmosphere.

Finally, our experiments showed that the metal could also be obtained separately in nitrogen (N_2) and hydrogen (5%) atmospheres. When 101.3 mg of $C_6H_6N_3[ReO_4]$ was thermally treated under nitrogen (N_2) at 350°C for 30 min, the resulted metal, labeled as Re metal 4, is shown to be amorphous (Figure 12). The crystallinity of the metal was improved when treated at 700 °C for 60 min (Re metal 4a). In a hydrogen atmosphere, the thermal decomposition of $C_6H_6N_3[ReO_4]$ at 700 °C for 60 min led to the formation of crystalline Re metal (Figure 13).

CONCLUSIONS

In summary, the present work investigated novel methods for Re metal production. This method is based on the use of a neutral organic compound, benzotriazole ($C_6H_5N_3$), for precipitation and use as a reducing agent for Re metal production. The metal obtained from various routes in this study was characterized and confirmed by powder X-ray diffraction peak broadening due to crystallite size, and lattice strain was analyzed by both Williamson−Hall and Debye−Scherrer methods. SEM analyses showed a porous texture on the surface of the metal, which could be attributed to the evolution of gaseous species during decomposition at high temperatures. SEM images were analyzed by ImageJ, which showed the average area and diameter of the pores are found to be 12.28 ± 5.78 μm^2 and 11.32 ± 5.77 μm, respectively. Efforts to duplicate these methods for the technetium are underway and results will be reported in due time.

EXPERIMENTAL SECTION

Preparation of $C_6H_6N_3[ReO_4]$. Benzotriazole (99% purity) was obtained from Alfa Aesar, whereas all other chemicals (≥99% purity) were obtained from Sigma-Aldrich. These chemicals were used as received without any further purification. The $C_6H_6N_3[ReO_4]$ salt was prepared following the method described in the literature[16,17] and characterized in solution (UV−visible spectroscopy) and in the solid state (powder X-ray diffraction; see Figure 1) prior to this study. All

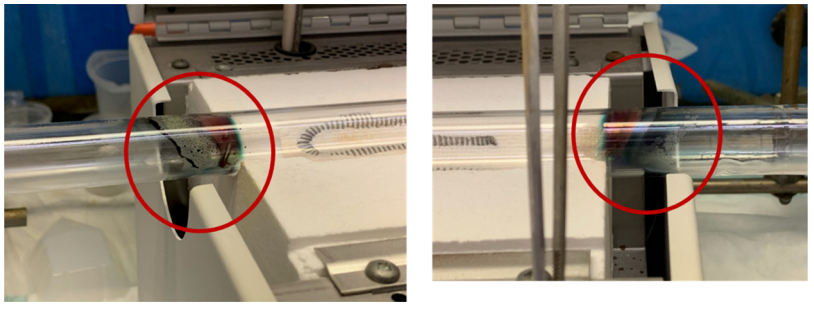

Figure 11. Photographic images taken by authors showing the formation of volatile rhenium species on both ends of the quartz tube following the thermal threat of $C_6H_6N_3[ReO_4]$ at 700 °C in air.

https://doi.org/10.1021/acsomega.1c04093
ACS Omega 2021, 6, 26672−26679

mixed powdered samples were prepared by pulverizing (3×) solid Re material and BTA ($C_6H_5N_3$) using a mortar and pestle at room temperature.

Thermal Analysis Measurements. Simultaneous thermal gravimetric analysis (TGA) and differential scanning calorimetry (DSC) measurements were performed in triplicate on crystalline $C_6H_6N_3[ReO_4]$ samples. TGA/DSC were performed on a NETZSCH STA 449 F1 Jupiter and data analyzed using NETZSCH Proteus software. The instrument was temperature and weight calibrated with a series of metal calibrants prior to sample analysis. Samples (≤25 mg) were scanned at a temperature rate of 10 K/min in an alumina crucible under argon with a purge rate of 20 mL/min.

Structural and Morphological Analyses. Powder X-ray diffraction (PXRD) measurements were performed using a Bruker D8 advanced diffractometer equipped with Cu Kα X-rays (1.5406 Å) and a solid-state Si detector. Samples were mounted on a low-background Si [1 1 1] disk sample holder. Powder XRD data were recorded from 2θ (10−90°) with a scanning rate of 0.010°/min. Powder XRD patterns were quantified by Rietveld analysis using Topas 4.0 software[37] and refined using appropriate crystal structures using a powder diffraction file (PDF) available from a crystallographic database (ICDD).

Scanning electron microscopy (SEM) and energy-dispersive X-ray (EDX) measurements were performed on JEOL model JSM-5610 equipment with secondary electron and backscattered electron. Data were analyzed using INCA Microanalysis Suite software v 4.15 and ImageJ v1.532.

■ ASSOCIATED CONTENT

Supporting Information

The Supporting Information is available free of charge at https://pubs.acs.org/doi/10.1021/acsomega.1c04093.

TGA/DSC of raw materials; decomposed materials in an argon atmosphere; and PXRD of mixed samples before and post heat treatment (PDF)

■ AUTHOR INFORMATION

Corresponding Authors

James Louis-Jean − *Department of Chemistry and Biochemistry, University of Nevada Las Vegas, Las Vegas, Nevada 89154, United States;* orcid.org/0000-0002-7711-0967; Email: louisjea@unlv.nevada.edu

Frederic Poineau − *Department of Chemistry and Biochemistry, University of Nevada Las Vegas, Las Vegas, Nevada 89154, United States*; Email: poineauf@unlv.nevada.edu

Authors

Harry Jang − *Department of Chemistry and Biochemistry, University of Nevada Las Vegas, Las Vegas, Nevada 89154, United States*

Andrew J. Swift − *Department of Chemistry and Biochemistry, University of Nevada Las Vegas, Las Vegas, Nevada 89154, United States; Physical and Life Sciences Directorate, Lawrence Livermore National Laboratory, Livermore, California 94550, United States;* orcid.org/0000-0002-7903-5032

Complete contact information is available at: https://pubs.acs.org/10.1021/acsomega.1c04093

Notes

The authors declare no competing financial interest.

■ ACKNOWLEDGMENTS

The authors thanks Julie Bertoia and Kelly Seeley for laboratory support, Dr. David W. Hatchett and Dr. Minghua Ren for instrumental support, and Jonathan George for technical assistance. This material is based upon the work performed under the auspices of the Consortium on Nuclear Security Technologies (CONNECT) supported by the Department of Energy/National Nuclear Security Administration under Award Number(s) DE-NA0003948. In addition, part of this material is based upon the work supported by the Department of Energy National Nuclear Security Administration through the Nuclear Science and Security Consortium under Award Number(s) DE-NA0003180. The Nuclear Regulatory Commission also supported part of this work (NRC Scholarship and Fellowship Program: NRC-HQ-84-15-G-21). This work was also performed under the auspices of the U.S. Department of Energy (DOE) by Lawrence Livermore National Laboratory (LLNL) under Contract No. DE-AC52−07NA27344.

■ REFERENCES

(1) Johnson, C. M.; Shirey, S. B.; Barovich, K. M. New Approaches to Crustal Evolution Studies and the Origin of Granitic Rocks: What Can the Lu-Hf and Re-Os Isotope Systems Tell Us? *Earth Environ. Sci. Trans. R. Soc. Edinburgh* **1996**, *87*, 339−352.

(2) Zhi, X. Re-Os Isotopic System and Formation Age of Subcontinental Lithosphere Mantle. *Chin. Sci. Bull.* **2000**, *45*, 193−200.

(3) Carlen, J. C.; Bryskin, B. D. Rhenium — A Unique Rare Metal. *Mater. Manuf. Process.* **1994**, *9*, 1087−1104.

(4) Kesieme, U.; Chrysanthou, A.; Catulli, M. Assessment of Supply Interruption of Rhenium, Recycling, Processing Sources and Technologies. *Int. J. Refract. Met. Hard Mater.* **2019**, *82*, 150−158.

(5) Louis-Jean, J.; Inglis, J. D.; Hanson, S.; Pollington, A.; Meininger, D.; Reilly, S.; Steiner, R. New Loading Method for High Precision Sm Isotope Analysis of Nuclear Materials Using Thermal Ionization Mass Spectrometry. *J. Radioanal. Nucl. Chem.* **2021**, *327*, 317−327.

(6) Noddack, W.; Tacke, I.; Berg, O. *Sitzber. Preuss. Akad. Wiss.* **1925**, *19*, 400−405.

(7) Noddack, V. W.; Tacke, I. Die Ekamangane. *Naturwissenschaften* **1925**, *13*, 567−574.

(8) Noddack, J.; Noddack, W. Die Herstellung von Einem Gram Rhenium. *Z. Anorg. Allg. Chem.* **1929**, *183*, 353−375.

(9) Greenwood, N. N.; Earnshaw, A. *Chemistry of the Elements*, 2nd ed.; Butterworth-Heinemann: Oxford, England, UK, 1997.

(10) Glemser, O. Ammonium Perrhenate. In *Handbook of Preparative Inorganic Chemistry*; Brauer, G., Ed.; Academic Press: New York, 1963; pp 1476−1485.

(11) Bryskin, B. D.; Danek, F. C. Powder Processing and the Fabrication of Rhenium. *JOM* **1991**, *43*, 24−26.

(12) Campbell, I. E.; Rosenbaum, D. M.; Gonser, B. W. The Availability, Recovery and Properties of Rhenium Metal. *J. Less-Common Met.* **1959**, *1*, 185−191.

(13) Anderson, C. D.; Taylor, P. R.; Anderson, C. G. Extractive Metallurgy of Rhenium: A Review. *Min., Metall., Explor.* **2013**, *30*, 59−73.

(14) Hurd, L. C.; Brimm, E.; Taebel, W. A.; Hopkins, B. S. Metallic Rhenium In *Inorganic Syntheses Vol. 1*; Booth, H. S., Ed.; McGraw-Hill, Inc.: New York, 1939; pp 175−178.

(15) Millensifer, T. A. Rhenium and Rhenium Compounds. In *Kirk-Othmer Encyclopedia of Chemical Technology*; John Wiley & Sons, Inc.: Hoboken, NJ, 2001; pp 1−21.

(16) Louis-Jean, J.; Jang, H.; Lawler, K. V.; Forster, P. M.; Ash, J.; Poineau, F. Preparation and Characterization of Benzotriazolium Perrhenate. *Inorg. Chim. Acta* **2019**, *498*, No. 119121.
(17) Louis-Jean, J.; Jang, H.; Lawler, K. V.; Swift, A. J.; Forster, P. M.; Ash, J.; Poineau, F. Benzotriazolium Metallate for 99Tc Immobilization and Remediation. *Trans. Am. Nucl. Soc.* **2020**, *123*, 128−129.
(18) Bai, M.; Liu, Z. H.; Zhou, L. J.; Liu, Z. Y.; Zhang, C. F. Preparation of Ultrafine Rhenium Powders by CVD Hydrogen Reduction of Volatile Rhenium Oxides. *Trans. Nonferrous Met. Soc. China* **2013**, *23*, 538−542.
(19) Sharif Javaherian, S.; Aghajani, H.; Tavakoli, H. Investigation on Ammonium Perrhenate Behaviour in Nitrogen, Argon and Hydrogen Atmosphere as a Part of Rhenium Extraction Process. *Miner. Process. Extr. Metall.* **2018**, *127*, 182−188.
(20) Katritzky, A. R.; Wang, Z.; Tsikolia, M.; Hall, C. D.; Carman, M. Benzotriazole Is Thermally More Stable than 1,2,3-Triazole. *Tetrahedron Lett.* **2006**, *47*, 7653−7654.
(21) Popova, I.; Yates, J. T. Adsorption and Thermal Behavior of Benzotriazole Chemisorbed on γ-Al2O3. *Langmuir* **1997**, *13*, 6169−6175.
(22) Poineau, F.; Hartmann, T.; Chinthaka Silva, G. W.; Jarvinen, G.; Czerwinski, K. Preparation of Technetium Metal by Thermal Treatment Under Argon/H2O. *J. Radioanal. Nucl. Chem.* **2009**, *279*, 43−48.
(23) Ohashi, M.; Tsujimoto, K.; Yoshino, A.; Yonezawa, T. Mass Spectra of Benzotriazoles. Correlation with Thermolytic and Photolytic Fragmentations. *Org. Mass Spectrom.* **1970**, *4*, 203−210.
(24) Shatynski, S. R. The Thermochemistry of Transition Metal Carbides. *Oxid. Met.* **1979**, *13*, 105−118.
(25) Gonzalez-Rodriguez, J.; Pepper, K.; Baron, M. G.; Mamo, S. K.; Simons, A. M. Production and Analysis of Recycled Ammonium Perrhenate from CMSX-4 Superalloys. *Open Chem.* **2018**, *16*, 1298−1306.
(26) Singh Gaur, R. P.; Wolfe, T. A.; Braymiller, S. A. Recycling of Rhenium-Containing Wire Scrap. *Int. J. Refract. Met. Hard Mater.* **2015**, *50*, 79−85.
(27) Mishra, S. K.; Roy, H.; Lohar, A. K.; Samanta, S. K.; Tiwari, S.; Dutta, K. A Comparative Assessment of Crystallite Size and Lattice Strain in Differently Cast A356 Aluminium Alloy. *IOP Conf. Ser.: Mater. Sci. Eng.* **2015**, *75*, No. 012001.
(28) Ahmadipour, M.; Abu, M. J.; Ab Rahman, M. F.; Ain, M. F.; Ahmad, Z. A. Assessment of Crystallite Size and Strain of CaCu3Ti4O12 Prepared via Conventional Solid-State Reaction. *Micro Nano Lett.* **2016**, *11*, 147−150.
(29) Khorsand Zak, A.; Abd Majid, W. H.; Abrishami, M. E.; Yousefi, R. X-Ray Analysis of ZnO Nanoparticles by Williamson-Hall and Size-Strain Plot Methods. *Solid State Sci.* **2011**, *13*, 251−256.
(30) Williamson, G. K.; Hall, W. H. X-Ray Line Broadening From Filed Aluminium and Wolfram. *Acta Metall.* **1953**, *1*, 22−31.
(31) Langford, J. I.; Wilson, A. J. C. Scherrer After Sixty Years: A Survey and Some New Results in the Determination of Crystallite Size. *J. Appl. Crystallogr.* **1978**, *11*, 102−113.
(32) Ivanovskii, A. L.; Chupakhina, T. I.; Zubkov, V. G.; Tyutyunnik, A. P.; Krasilnikov, V. N.; Bazuev, G. V.; Okatov, S. V.; Lichtenstein, A. I. Structure and Electronic Properties of New Rutile-Like Rhenium (IV) Dioxide ReO2. *Phys. Lett. A* **2005**, *348*, 66−70.
(33) Childs, B. C.; Braband, H.; Lawler, K.; Mast, D. S.; Bigler, L.; Stalder, U.; Forster, P. M.; Czerwinski, K. R.; Alberto, R.; Sattelberger, A. P.; et al. Ditechnetium Heptoxide Revisited: Solid-State, Gas-Phase, and Theoretical Studies. *Inorg. Chem.* **2016**, *55*, 10445−10452.
(34) Childs, B. C. Volatile Technetium Oxides: Implications for Nuclear Waste Vitrification, UNLV Theses, Diss. Prof. Pap. Capstones, 2017.
(35) Childs, B. C.; Poineau, F.; Czerwinski, K. R.; Sattelberger, A. P. The Nature of the Volatile Technetium Species Formed During Vitrification of Borosilicate Glass. *J. Radioanal. Nucl. Chem.* **2015**, *306*, 417−421.
(36) Childs, B. C.; Lawler, K. V.; Braband, H.; Mast, D. S.; Bigler, L.; Stalder, U.; Peterson, D. R.; Jansen, A.; Forster, P. M.; Czerwinski, K. R.; et al. The Nature of the Technetium Species Formed During the Oxidation of Technetium Dioxide with Oxygen and Water. *Eur. J. Inorg. Chem.* **2018**, *2018*, 1137−1144.
(37) Topas V2.0.*Profile and Structure Analysis Software for Powder Diffraction Data.*; Bruker AXS: Karlsruhe: Germany, 2000.

https://doi.org/10.1021/acsomega.1c04093
ACS Omega 2021, 6, 26672−26679